Measurement 44 (2011) 2194–2199

Contents lists available at ScienceDirect

Measurement

journal homepage: www.elsevier.com/locate/measurement

Characterization of thermoelectric generators by measuring the load-dependence behavior

J.P. Carmo *, Joaquim Antunes, M.F. Silva, J.F. Ribeiro, L.M. Goncalves, J.H. Correia

Univ. of Minho, Dept. Industrial Electronics, Campus Azurem, 4800-058 Guimaraes, Portugal

ARTICLE INFO

Article history:
Received 7 January 2011
Received in revised form 29 June 2011
Accepted 18 July 2011
Available online 2 August 2011

Keywords:
Measurement
Data acquisition
Thermoelectric generator
Seebeck effect
Power source characterization
Measurement setup

ABSTRACT

Solid-state thermoelectric generators (TEGs) based on the Seebeck effect to convert temperature gradients, ΔT [K], into electrical energy are being used in an increased number of stand-alone microsystems applications. These generators are composed by at least one pair of *p*- and *n*-type thermoelectric elements with high figures-of-merit, *ZT*, to perform such a conversion. The exact behavior knowledge of generators is mandatory in order to decide the most suitable for the target application. The focus of this paper is to present a methodology to characterize thermoelectric generators, by measuring their behavior for different types of loads. The measurements were done with the help of commercial thermoelectric generators (thermoelectric modules TEC1-12707) and a measurement setup composed by a controlled hot-plate, a controlled cooling fan (above an heat dissipator), a set of two thermistors for measuring the temperature, a personal computer with the data acquisition board model NI USB-6009 and the LabView software from National Instruments for acquiring the measures and for controlling both the hot-plate and the cooling fan. The thermoelectric modules TEC1-12707 was selected due to its compact size (e.g., 40 mm × 40 mm) and because it can withstand temperatures up to 450 K without degrading the quality of measurements. A SPICE model for thermoelectric modules TEC1-12707 was also obtained: an open-circuit voltage of $V_{open} = 53.17 \times \Delta T$ [mV] and an internal resistance of $R_0 = 3.88\ \Omega$ with a tolerance of $\Delta R_{int} = 0.13\ \Omega$ such that $R_{int} = R_0 \pm \Delta R_{int} = 3.88 \pm 0.13\ \Omega$. The measurements done under the maximum output power delivery condition (for the maximum temperature gradient of $\Delta T = 51$ °C) resulted in the maximum output power of $P_{out} = 500$ mW, as well as in the output current and voltage of $I_{out} = 357$ mA and $V_{out} = 1.40$ V, respectively. The load resistance of 3.92 Ω (V_{out}/I_{out}) is also in accordance with the measurements because it is located in the range $[\mu - \sigma,\ \mu + \sigma]\ \Omega$, where $\mu = R_0 = 3.88\ \Omega$ and $\sigma = \Delta R_{int} = 0.13\ \Omega$. An Agilent multimeter model 34410A with 6½ digits was used for measuring the voltages at the TEG's output and the respective currents.

1. Introduction

In the present days there is the increased concern to reduce fossil fuel dependence because it is necessary to revert their effects on the environment, e.g., reduction in the ozone depletion or greenhouse effect due to the gas emissions [1,2]. In this context, the use of renewable sources of power is a concern even more and more high [3–6]. The development of the materials technology reached a matured phase where the idea of fabricating all solid-state thermoelectric generators was possible to achieve [7–10]. A solid-state thermoelectric generator is a device that converts temperature gradients into electricity and whose components do not include neither any type of movable parts nor any kind of fluids (for example, Freon gaz) [11,12] which makes these type of converters very appreciated for stand-alone nodes of wireless sensors networks with harvesting capabilities [10,13–15] for running at large

* Corresponding author. Tel.: +351 253 510190; fax: +351 253 510189.
E-mail address: jcarmo@dei.uminho.pt (J.P. Carmo).

0263-2241/$ - see front matter © 2011 Elsevier Ltd. All rights reserved.
doi:10.1016/j.measurement.2011.07.015

periods of time with battery replacement and/or node management [16–19]. In fact, solid-state thermoelectric converters are generally based on heavily doped semiconductors use the Seebeck effect to produce electrical energy [20,21]. In a general form, the performance of a TE device is determined by the figure-of-merit of the materials used [21–31], which is expressed in terms of the dimensionless parameter, ZT, given by:

$$ZT = \alpha^2 T/(\rho\kappa) \quad (1)$$

where α [V K^{-1}] is the Seebeck coefficient, ρ [Ωm] is the electrical resistivity, κ [Wm^{-1} K^{-1}] is the thermal conductivity and T [K] the temperature. The performance parameter ZT is very useful in Seebeck sensing devices, such as infrared thermal detectors. In a thermoelectric converter, another performance factor is more appropriate, which is the power-factor, PF [WK^{-2} m^{-1}]. The PF is defined as the electric power per unit of area through which the heat flows, per unit of temperature gradient between the hot and the cold sides, and is expressed as:

$$PF = \alpha^2/\rho \quad (2)$$

In this context, this paper presents a measurement methodology for characterizing the behavior and the performance of thermoelectric converters. A set of commercial modules were used to achieve such a purpose. The thermoelectric modules model TEC1-12707 presents a contact area of 40 mm by 40 mm and can work with temperatures up to 450 K without taking the risk to degrade the quality of the measurements and thus, putting in jeopardize the applicability of the proposed method.

2. Measurement setup

The Fig. 1a shows an artist impression of a typical thermoelectric converter and the respective physical factors that determine its operation. If the junctions at the bottom are heated and those at the top are cooled (producing a temperature differential) then electron/hole pairs will be created at the hot end and absorb heat in the process. The pairs recombine and reject heat at the cold ends. A voltage potential, the Seebeck voltage, which drives the hole/electron flow, is created by the temperature difference between the hot and cold ends of the thermoelectric elements. The net voltage appears across the bottom of the thermoelectric element legs. The photography in the Fig. 1b shows a thermoelectric module model TEC1-12707 already encapsulated (and for this reason, the thermoelectric pairs are not visible).

The measurement setup showed in the Fig. 2 takes in account the shape of this thermoelectric converter by mounting one of the faces above a controlled hot-plate and letting the totality of the other face touching a controlled cooling fan. Additionally, two cooper plates were placed on both sides of the thermoelectric converter in order to improve the thermal contact with the hot-plate and cooling fan. This arrangement favors the precise control of the heat flow and thus, the precise measurement of the temperature on both sides by way of a set of two thermistors connected to a bridge of resistors. The program for measuring and controlling both the hot-plate and the cooling fan was implemented with the help of LabView language for interfacing with the National Instruments data acquisition board model NI USB-6009. The reasons behind the selection of this data acquisition board was its low-cost with reasonable specifications for the application proposed in this paper. The USB interface makes this data acquisition board especially targeted for fast application prototyping at low cost and at the same time it allows the simultaneous acquisition of two signals with a resolution of fourteen bits and a speed of 24 K samples per second. Two digital outputs were used for controlling the power electronics module responsible for supplying the hot-plate and the cooling fan.

The procedure used for characterization of the converters was as follows: The hot-plate temperature and the cooling fan exhaustion were adjusted in order to keep the heat flow constant for several resistive loads connected to the output of the thermoelectric converter. This was done by implementing two closed-loops controlling systems with the help of the two thermistors on both sides of the thermoelectric converter. This controlling scheme allowed the trimming of both the hot-plate and cooling fan set-points in order to maintain constant the temperatures in the both sides of the converter. After adjusting the temperature gradient, the load is connected and a new temperature adjustment is done in order to provide the same temperature gradient as before. This is because the heat flow will depend on the electric current and thus, a new temperature gradient will be present and must be adjusted to the original value before the load connection. Six test temperatures (T_{test} = 50, 80, 120, 150, 180, 195 °C) were used for generating six temperature gradients ($\Delta T = T_H - T_C$ = 8, 13, 30, 37, 47, 75 °C, T_H and T_C are the temperatures on the hot and cold sides respectively) in order to test the thermoelectric converters and characterize their behavior. The Table 1 shows the several temperatures involved on measurements, where it can be observed that for a given (and fixed) test temperature, T_{test} [°C], there is a ON/OFF temperature range on the hot-plate, T_{ON}/T_{OFF} [°C], to ensure (with the help of the cooling fan) that the temperature on the both sides of the thermoelectric converter are fixed and kept equal to T_H and T_C [°C].

After adjusting the test temperature, T_{test}, the LabView program keeps constant the temperature gradient, $\Delta T = T_H - T_C$, (presented above) in order to measure the voltage at the output of thermoelectric generator, V_{out} [mV], and the respective current, I_{out} [mA]. Measurement pairs of the voltage and current, {V_{out}, I_{out}}, are acquired while the load resistance, R_{load} [Ω], is manually adjusted. This manual procedure is necessary for getting all the necessary data for doing the plots presented further (e.g., V_{out}, I_{out}, P_{out}, R_{load} and R_{int}). The internal resistance, R_{int} [Ω], of the thermoelectric generator is calculated as follows: $R_{int} = V_{open}/I_{short}$, where V_{open} [mV] is the open-circuit voltage and I_{short} [mA] is the short-circuit current. All voltages and currents were measured using an Agilent multimeter model 34410A with 6½ digits. The maximum voltage error is {3 μV, 6 μV, 40 μV} for voltages smaller than {100 mV, 1 V, 10 V}, respectively; while the maximum current error is {40 μA, 60 μA, 0.6 mA} for currents smaller than

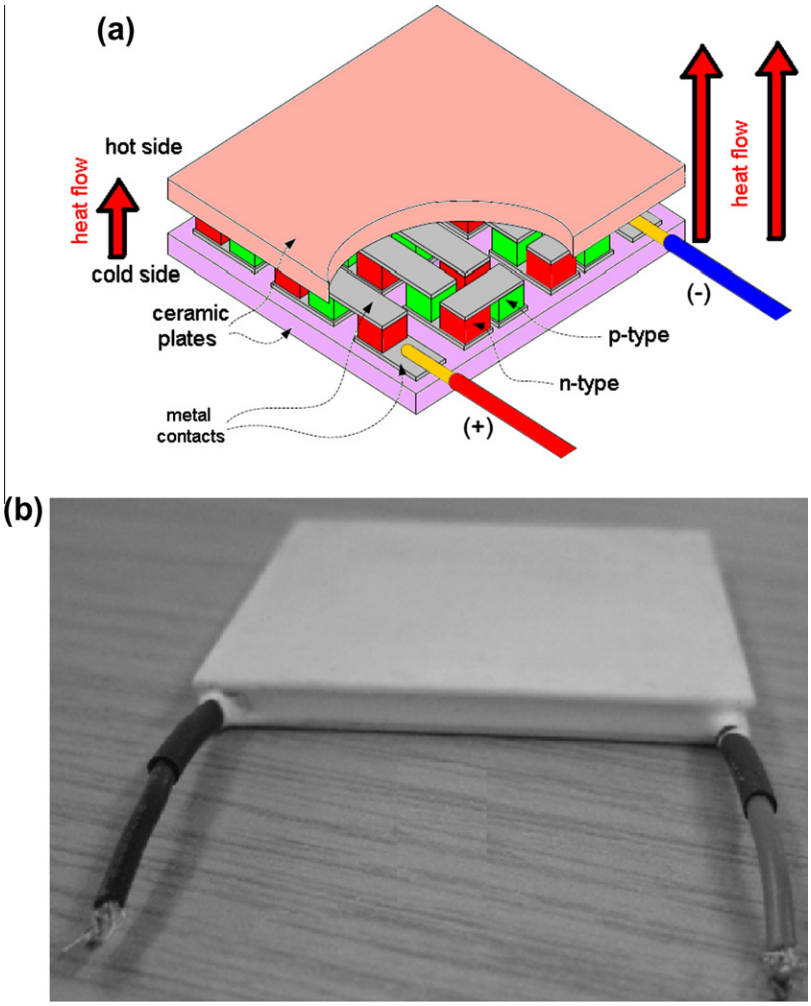

Fig. 1. (a) Artwork of a thermoelectric converter, where it can be seen that when the heat flows across the junction, an electrical power current is generated through the Seebeck effect. It can also be observed that practical thermoelectric generators (it is the illustrated case) connect large number of junctions in series to increase the operating voltage and to better spread the heat flow. [27]. (b) Photography of a fully encapsulated thermoelectric module model TEC1-12707.

{100 mA, 1 A, 3 A} under voltages smaller than {0.3 V, 0.8 V, 2 V}, respectively. These errors were calculated taking in account the full-range error obtained from the operation manual of the Agilent manufacturer [32]. This multimeter was also used for measuring the short-circuit currents because the output voltage was always smaller than the most restrictive acceptable value, e.g., 0.3 V.

3. Experimental results

The first set of tests consisted in the determination of the V/I (output voltage versus the output current) output characteristic of the thermoelectric converter. The Fig. 3 shows the output voltage, V_{out} [mA], versus the output current, I_{out} [mA], for several test temperatures, T_{test} [°C], and thus, for several temperature gradients, $\Delta T = T_H - T_C$ [°C]. As expected (and the same conclusion applies to the load-less case), the output voltage increases with the test temperature, T_{test}, (and thus, with the temperature gradient, ΔT). This conclusion is valid for the plot of the Fig. 3 and for similar plots, since the test temperatures are such that the thermoelectric converter is not behind a certain thermal saturation point. It can be observed a high linearity in all V/I plots and almost the same slope. This means that the internal resistance of the thermoelectric converter still constant with the test temperature and load operations. From these V/I output characteristics it is thus possible to obtain the internal resistance of the device – see the Fig. 4. It is possible to observe the clear existence of clusters for a given test temperature. In order to determine the statistical behavior of these clusters, it was calculated their medium ($\mu_i \in 3.51,\ 3.81,\ 4.37,\ 4.04,\ 4.04,\ 3.50\ \Omega$) and standard deviation ($\sigma_i \in 0.42,\ 0.33,\ 0.26,\ 0.37,\ 0.37,\ 0.07\ \Omega$) values as showed in the Fig. 5. Excepting for the case of the test temperature of 195 °C, the length of the intervals (the standard deviation) around the center values of the clusters (their medium) can be considered to have the same order of magnitude. This indicates a repetition

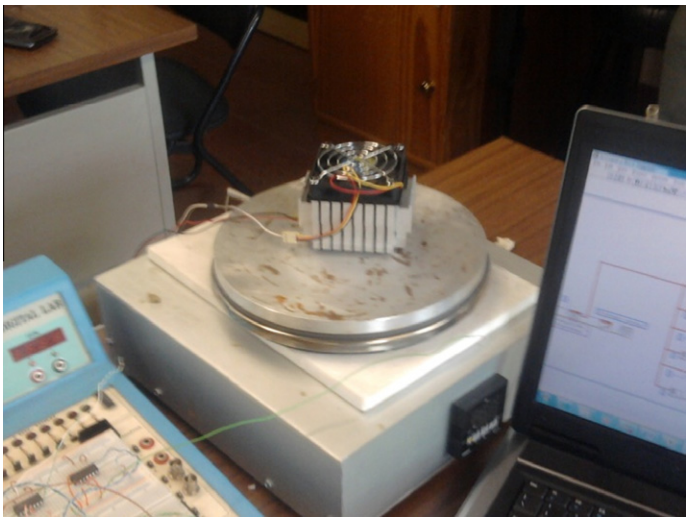

Fig. 2. The measurement setup showing a thermoelectric modules model TEC1-12707 between a controlled hot-plate and a controlled cooling fan. The personal computer running the LabView software connects to a data acquisition board model NI USB-6009 for controlling the heat flow (by way of the controlled hot-plate and the cooling fan) and for measure the produced currents and the respective voltages.

Table 1
The several temperatures involved on the measurements and the output voltage of the thermoelectric converter in the absence of any electrical load connected to it.

Test temperature, T_{test} (°C)	Control temperature, T_{ON}–T_{OFF} (°C)	Hot temperature, T_H (°C)	Cold temperature, T_C (°C)	Temperature gradient, ΔT (°C)	Open-circuit voltage, V_{open} (mV)
50	49.9–51	47	39	8	400
80	79.9–82.2	62	49	13	810
120	118–121	80	50	30	1450
150	148–150.5	98	61	37	1970
180	177.8–180.2	117	70	47	2430
195	191.5–196	126	75	51	2630

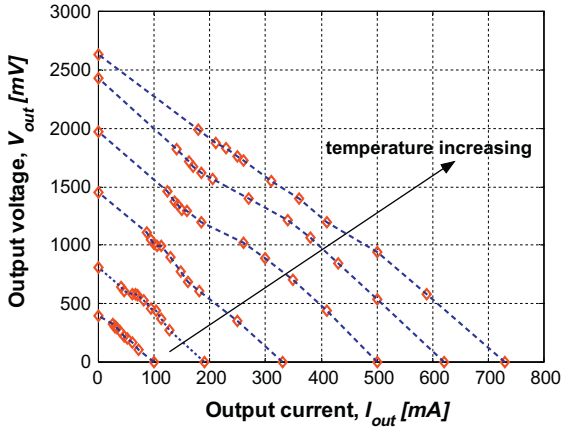

Fig. 3. The output voltage, V_{out} [mA], versus the output current, I_{out} [mA], for several test temperatures, T_{test} [°C].

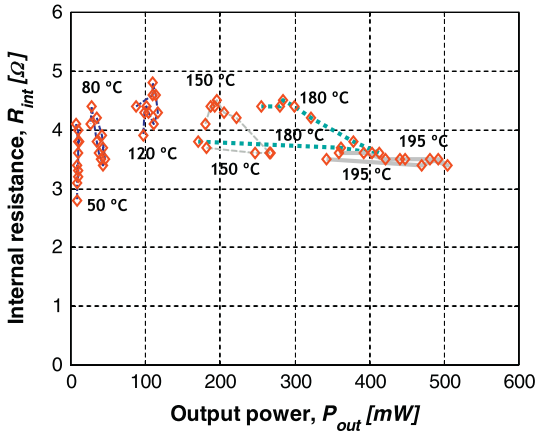

Fig. 4. The internal resistance of thermoelectric converter, R_{int} [Ω], versus the output power, P_{out} [mW], for several test temperatures, T_{test} [°C].

of a certain pattern on the behavior of the thermoelectric converter. The possible explanation for this discrepancy is the variability of the measuring conditions due to the high test temperature involved in the characterization process (e.g., calorimetric leaks around the hot-plate, a difficulty to guarantee the hot-plate and cooling fan set-points and/or more difficulties to dissipate the heat on

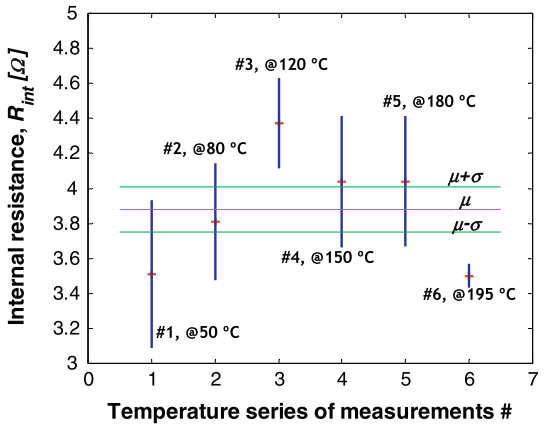

Fig. 5. The medium and standard deviation values of the internal resistance of the thermoelectric converter, R_{int} [Ω], versus the output power, P_{out} [mW], for all the test temperatures, T_{test} [°C].

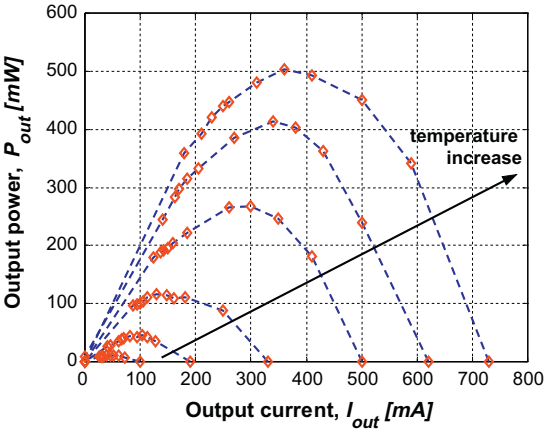

Fig. 6. Output power, P_{out} [mW], versus the output current, I_{out} [mA] for the six test temperatures.

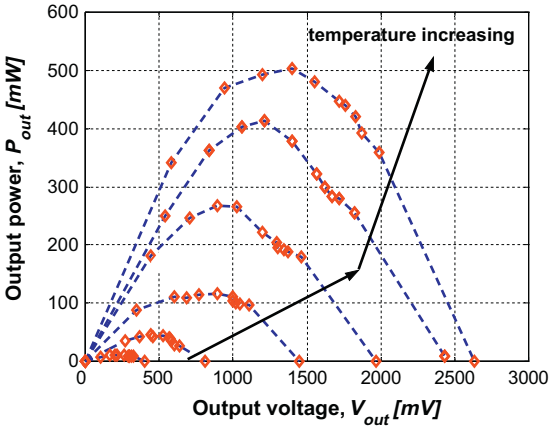

Fig. 7. Output power, P_{out} [mW], versus the output voltage, V_{out} [mA] for the six test temperatures.

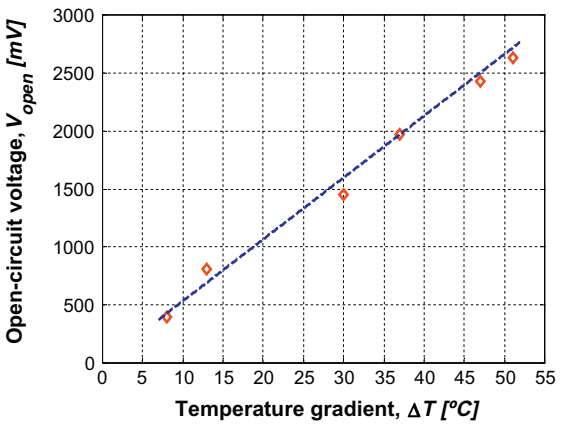

Fig. 8. The open-circuit voltage, V_{open} [mV], as function of the temperature gradient, ΔT [°C].

the dissipation that resulted of the convection from the hot-plate). The central line of the three horizontal lines represents the medium of the mediums (e.g., $\mu = [\mu_1 + \mu_2 + \mu_3 + \mu_4 + \mu_5 + \mu_6]/6 \approx 3.88\ \Omega$), while the equal distances between this central line (μ) to the top and the bottom lines is the standard deviation of the standard deviations (σ = standard deviation of the set σ_1, σ_2, σ_3, σ_4, σ_5, $\sigma_6 \approx 0.13\ \Omega$). These last two lines are located on $\mu + \sigma$ and $\mu - \sigma$, respectively. From this analysis, it possible to conclude that the internal resistance of the analyzed thermoelectric device is equal to $R_0 = 3.88\ \Omega$, with a tolerance equal to $\Delta R_{int} = 0.13\ \Omega$, thus, $R_{int} = R_0 \pm \Delta R_{int} = 3.88 \pm 0.13\ \Omega$.

An analysis to both plots of the Figs. 3 and 4 allows the observation of an increasing in the output power, P_{out} [mW], with the test temperatures. The explanation for this observation results from the rise of the temperature gradient, ΔT [°C], whose consequence is an increase in the output voltage, V_{out} [mV]. As high is this output voltage, the high will be the output current (for a given load resistance, R_L [Ω]) and therefore will be the dissipated power in the external load, e.g. $P_{out} = R_L I_{out}$ [mW]. Taking this in account, and considering several values for the load resistance, it was also possible to obtain the Fig. 6 for the output power, P_{out} [mW], versus the output current, I_{out} [mA] (or versus the load resistance, R_L [Ω]). It must be noted that as it happened with the Fig. 3, this one also illustrates six plots for the six test temperatures. The Fig. 7 is an alternative set of plots, but for the output power, P_{out} [mW], versus the output voltage, V_{out} [mA] and once again for the six test temperatures.

The analysis done to the open-circuit voltage, V_{open} [mV], measured at the output of the thermoelectric converter allowed to plot the graph of the Fig. 8 as function of the temperature gradient, ΔT [°C]. A quadratic minimization was applied to the points of the graph of the Fig. 8, and the following open-voltage function was obtained:

$$V_{open} = 53.17 \times \Delta T[mV] \quad (3)$$

This open-voltage function in conjunction with the internal resistance of the thermoelectric converter formerly obtained allows the definition of a SPICE model of an equivalent controlled (by the temperature gradient) voltage source for use in circuit simulations, where the behavior of the power source must be taken in account.

4. Conclusions

This paper presented a method for characterizing the behavior of thermoelectric converters. The method is based on measuring the voltages and currents supplied by the thermo-converter as a response to variations of the load resistance. It was used thermoelectric modules model TEC1-12707 for doing the measurements and the characterization of this device. In spite of being used a commercial thermoelectric converter, the method can be applied to other thermoelectric modules that use the Seebeck effect to convert temperature differences (or temperature gradients) to voltages (and thus, to supplied currents to certain resistive loads). The obtained models can be used on simulation tools that use SPICE parameters. The main model of the thermoelectric converters is composed by an ideal voltage source in series with an internal resistance. The open-circuit voltage V_{open} [mV] at the output of the thermoelectric converter depends only from the temperature gradient ΔT [°C] (e.g., with $V_{open} = K \times \Delta T$ – obviously $V_{open} = 0$ V for $\Delta T = 0$ °C) whereas the internal resistance is intrinsic to the thermoelectric converter. Moreover, this serial resistance has a given tolerance that is also intrinsic to the thermoelectric converter, e.g., $R_{int} = R_0 \pm \Delta R_{int}$. The measurements done on the thermoelectric modules model TEC1-12707 resulted on the following SPICE parameters: $V_{open} = 53.17 \times \Delta T$ [mV] and $R_{int} = 3.88 \pm 0.13\ \Omega$.

References

[1] L.E. Bell, Cooling, heating, generating power, and recovering waste heat with thermoelectric systems, Science 321 (September) (2008) 1457–1461.

[2] R.F. Service, Temperature rises for devices that turn heat into electricity, Science 306 (October) (2004) 806–807.

[3] J.M. Carrasco, J.M. Carrasco, L.G. Franquelo, J.T. Bialasiewicz, E. Galvan, R.C.P. Guisado, Ma.A.M. Prats, J.L. Leon, N. Moreno-Alfonso, Power-electronic systems for the grid integration of renewable energy sources: a survey, IEEE Transactions on Industrial Electronics 53 (4) (2006) 1002–1016.

[4] J. Schonbergerschonberger, R. Duke, S.D. Round, DC-bus signaling: a distributed control strategy for a hybrid renewable nanogrid, IEEE Transactions on Industrial Electronics 53 (5) (2006) 1453–1460.

[5] R.J. Wai, W.H. Wang, C. Lin, C. Li, High-performance stand-alone photovoltaic generation system, IEEE Transactions on Industrial Electronics 55 (1) (2008) 240–250.

[6] J. Colomer-Ferrarons, P. Miribel Català, A. Saiz Vela, M. Puig Vidal, J. Samitier, Power-conditioning circuitry for a self powered system based on micro PZT generators in a 0.13 um low voltage low-power technology, IEEE Transactions on Industrial Electronics 55 (9) (2008) 3249–3257.

[7] Z.H. Zhenga, P. Fan, G.X. Lianga, D.P. Zhanga, X.M. Caia, T.B. Chena, Annealing temperature influence on electrical properties of ion beam sputtered Bi_2 Te_3 thin films, Journal of Physics and Chemistry of Solids 71 (December) (2010) 713–1716.

[8] D. Pinisettya, R.V. Devireddy, Thermal conductivity of semiconductor (bismuth-telluride)-semimetal (antimony) superlattice nanostructures", Acta Materialia 58 (January) (2010) 570–576.

[9] J.P. Carmo, L.M. Goncalves, J.H. Correia, Improved p-, Improved *p*- and *n*-type thin-film microstructures for thermoelectricity, Electronic Letters 45 (July) (2009) 803–805.

[10] J.P. Carmo, L.M. Goncalves, J.H. Correia, Thermoelectric microconverter for energy harvesting systems, IEEE Transactions on Industrial Electronics 57 (March) (2010) 861–867.

[11] B. Poudel, Q. Hao, Y. Ma, Y. Lan, A. Minnich, B. Yu, X. Yan, D. Wang, A. Muto, D. Vashaee, X. Chen, J. Liu, M.S. Dresselhaus, G. Chen, Z. Ren, High-thermoelectric performance of nanostructured bismuth antimony telluride bulk alloys, Science 320 (May) (2008) 634–638.

[12] C.B. Vining, Semiconductors are cool, Nature 413 (October) (2001) 577–578.

[13] R.F. Yazicioglu, T. Torfs, P. Merken, J. Penders, V. Leonov, R. Puers, B. Gyselinkx, C.V. Hoof, Utra-low-power biopotential interfaces and their applications in wearable and implantable systems, Microelectronics Journal Science 40 (September) (2009) 1313–1321.

[14] V. Leonov, R.J.M. Vullers, Wearable electronics self-powered by using human body heat: the state of the art and the perspective, Journal of Renewable and Sustainable Energy 1 (2009) 1–14. 062701.

[15] H. Yousef, K. Hjort, M. Lindeberg, Vertical thermopiles embedded in a Polyimide-based flexible printed circuit board, Journal of Microelectromechanical Systems 16 (September) (2007) 1341–1348.

[16] M. Armand, J.M. Tarascon, Building better batteries, Nature 451 (February) (2008) 652–657.

[17] L. Mateu, F. Moll, Appropriate charge control of the storage capacitor in a piezoelectric energy harvesting device for discontinuous load operation, Journal of Sensors and Actuators A 132 (2006) 302–310.

[18] H. Nishide, K. Oyaizu, Toward flexible batteries, Science 319 (February) (2008) 737–738.

[19] J.P. Carmo, J.F. Ribeiro, M.F. Silva, L.M. Goncalves, J.H. Correia, Thermoelectric generator and solid-state battery for stand-alone microsystems, Journal of Micromechanics and Microengineering 20 (8) (2010) 1–8.

[20] K.F. Hsu, S. Loo, F. Guo, W. Chen, J.S. Dyck, C. Uher, T. Hogan, E.K. Polychroniadis, M.G. Kanatzidis, Cubic AgPb $_m$SbTe$_{2+m}$ bulk thermoelectric materials with high figure of merit, Science 303 (February) (2004) 818–821.

[21] E. Vremera, L. Brunetti, L. Oberto, M. Sellone, Alternative procedures in realizing of the high frequency power standards with microcalorimeter and thermoelectric power sensors, Measurement 42 (February) (2009) 269–276.

[22] B. Sokolov, S.Y. Skipidarova, N.I. Duvankova, G.G. Shabuninab, Chemical reactions on the Bi_2 Te_3 –Bi_2 Se_3 section in the process of crystal growth, Journal of Crystal Growth 262 (2004) 442–448.

[23] J. Jiang, L. Chen, S. Bai, Q. Yao, Q. Wang, Thermo-electric properties of *p*-type crystals prepared via zone melting, Journal of Crystal Growth 277 (2005) 258–263.

[24] R. Venkatasubramanian, E. Siivola, T. Colpitts, B. O'Quinn, Thin-film thermo-electric devices with high room-temperature figures of merit, Nature 413 (October) (2001) 597–602.

[25] D.D.L. Wijngaards, R.F. Wolffenbuttel, Thermo-electric characterization of APCVD poly$Si_{0.7}Se_{0.3}$ for IC-compatible fabrication of integrated lateral Peltier elements, IEEE Transactions on Electron Devices 52 (5) (2005).

[26] L.W. da Silva, K. Massoud, Citrad Uher, Thermo-electric performance of films in the Antimony-tellurium and antimony-tellurium systems, Journal of Applied Physics 97 (2005).

[27] M.F. Silva, Thin-films for thermoelectric applications, MSc Thesis on Micro/Nanotechnologies, University of Minho, November 2010.

[28] B. Huang, C. Lawrence, A. Gross, G.S. Hwang, N. Ghafouri, S.W. Lee, H. Kim, C.P. Li, C. Uher, K. Najafi, M. Kaviany, Low-temperature characterization and micro-patterning of co-evaporated Bi_2Te_3 and Sb_2Te_3 films, Journal of Applied Physics 104 (2008) 113710.

[29] I. Boniche, B.C. Morgan, P.J. Taylor, C.D. Meyer, D.P. Arnold, Process development, Process development and material characterization of polycrystalline Bi_2Te_3, PbTe, and PbSnSeTe thin films on silicon for millimeter-scale thermoelectric generators, Journal of Vacuum Science and Technology A 26 (2008) 739–744.

[30] M.V. Kovalenko, B. Spokoyny, J.-S. Lee, M. Scheele, A. Weber, S. Perera, D. Landry, D.V. Talapin, Semiconductor nanocrystals functionalized with antimony telluride Zintl ions for nanostructured thermoelectrics, Journal of the American Chemical Society 132 (2010) 6686–6695.

[31] M.Y. Kim, T.S. Oh, Thermoelectric characteristics of the thermopile sensors with variations of the width and the thickness of the electrodeposited bismuth-telluride and antimony-telluride thin films, Materials Transactions 51 (2010) 1909–1913.

[32] Agilent Technologies, 34410A digital multimeter 6½ digit high performance. <http://www.agilent.com/>.